Journal of Applied Mechanics. Received March 27, 2023;
Accepted manuscript posted April 15, 2023. doi:10.1115/1.4062389

An Entropy Dynamics Approach for Deriving and Applying Fractal and Fractional Order Viscoelasticity to Elastomers

Basanta R. Pahari
Department of Mechanical Engineering
Florida A&M University and Florida State University
Tallahassee, FL 32310
Email: bpahari@fsu.edu

Eugenia Stanisauskis
Department of Materials Science
Florida State University
Tallahassee, FL 32306
Email: estanisauskis@fsu.edu

Somayeh Mashayekhi
Department of Mathematics
Kennesaw State University
Marietta, GA 30060
Email: smashay1@kennesaw.edu

William Oates
Department of Mechanical Engineering
Florida A&M University and Florida State University
Tallahassee, FL 32310
Email: woates@eng.famu.fsu.edu

Entropy dynamics is a Bayesian inference methodology that can be used to quantify time-dependent posterior probability densities that guide development of complex material models using information theory. Here we expand its application to non-Gaussian processes to evaluate how fractal structure can influence fractional hyperelasticity and viscoelasticity in elastomers. We investigate how kinematic constraints on fractal polymer network deformation influences the form of hyperelastic constitutive behavior and viscoelasticity in soft materials such as dielectric elastomers which have applications in the development of adaptive structures. The modeling framework is validated on two dielectric elastomers, VHB 4910 and 4949, over a broad range of stretch rates. It is shown that local fractal time derivatives are equally effective at predicting viscoelasticity in these materials in comparison to non-local fractional time derivatives under constant stretch rates. We describe the origin of this accuracy which has implications for simulating larger scale problems such as finite element analysis given the differences in computational efficiency of non-local fractional derivatives versus local fractal derivatives.

1 INTRODUCTION

Constitutive model development for polymeric materials traditionally starts with a free energy function that contains information about the internal energy of the bonds between atoms and the entropy governing heat transport and the configurations of the polymer network as a function of macroscopic deformation [1, 2, 3]. Information about the internal degrees of freedom that span quantum, molecular, mesoscale, and macroscales remains extraordinarily difficult to explicitly quantify and therefore techniques that use entropy to quantify measures of uncertainty are important to approximate internal forces and transport phenomena (e.g., heat transport, chemical diffusion, photochemistry, etc.) without complete knowledge across all scales. It was rather fortuitous that the pioneering work by Shannon's theory of information [4] was useful in modeling thermodynamic entropy [5, 6]. In this work, we use the tools from information theory to better understand the nonlinear, rate-dependent mechanics of elastomers that exhibit complexity which we encode as fractals or multifractals (random fractals) [7]. We do this by using entropy dynamics [8] and modifying the framework to include fractional constraints which restricts multiscale material structure to move along fractal dimensions. We relate fractal and fractional order operators to fractal structure to construct models that more accurately predict nonlinear, rate-dependent deformation in elastomers guided by an entropy dynamic framework.

The field of fractals and fractional order operators to

Journal of Applied Mechanics. Received March 27, 2023;
Accepted manuscript posted April 15, 2023. doi:10.1115/1.4062389

materials science is extensive and has grown significantly in the past several years. Seminal works in the broader field of fractional calculus [9, 10] and fractal diffusion in materials [11, 12] have motivated more recent efforts to understand how both fractal and fractional order operators provide new insights into complex material behavior [13, 14, 15, 16, 17, 18, 19, 20]. Mandelbrot's concept of fractals [21] provides a measure of 1D, 2D, and 3D geometry or time series characteristics that are otherwise difficult to quantify on a finite domain. For example, the circumference of an island can be infinitely long given a repeated (fractal) structure over all length scales. These measures are made finite on a fractal domain. In terms of time scales, fractal behavior manifest in terms of rates of change of some physical property such as velocity which may follow a fractal response as the kinetic behavior of a material is viewed on different time scales. This fractal mathematical property is defined over all length scales which serves as an approximate model of a material with finite bounds in space and time. Upper and lower limits of the fractal domain have been considered to address these finite length scales [22, 23, 15].

We focus on constitutive relations near equilibrium while accommodating dissipation characterized by viscoelasticity. Elastomers exhibit complexities due to the vast number of polymer network configurations that result in nonlinear deformation and thermal dissipation upon time dependent deformation. These complexities across molecular to continuum scales remain challenging as error propagation limits prediction across a broad range of deformation states and long time periods. In the limiting case of Gaussian processes, approximations can be made to develop idealized constitutive relations that lead to the very well known neo-Hookean model of hyperelasticity [2, 3]. Beyond moderate strain levels, elastomers exhibit nonlinearities characterized by non-Gaussian processes. Phenomenological methods can accommodate these nonlinearities in the stress-stretch behavior such as the Mooney-Rivlin and Ogden models [2]. However, these models are limited by their phenomenological nature requiring parameter estimation from data that is not well informed by the polymer structure. Other modeling approaches accommodate polymer structure and microscopic effects of polymer entanglement, cross-linking and non-affine deformation [24, 25]. These models make assumptions on the microscopic volume elements that are homogenized over a continuum volume. Although these models have been successful in predicting finite deformation in certain elastomers, homogenization across continuum scales is based on a limited number of microscopic factors that often ignore non-Gaussian statistical distributions, direct relations to multiscale structure, and connections to viscoelasticity. In many cases, fat-tailed probability distributions of polymer molecular motion becomes important and the fractal nature of materials can provide inputs to more accurately reflect derivative operations in the continuum scale constitutive model. This can have a significant influence on macroscale constitutive behavior as extreme events in the tails of the probability densities can have a cascading influence on macroscopic thermodynamic and kinetic properties.

West and Grigolini have argued that fractal structure is often best approximated by fractional calculus operators [9]. The pervasive nature of fractal structures in nature, including materials, clearly illustrates a unique opportunity to understand how to apply these operators to develop constitutive relations in complex materials. One striking example is the fractional form of the continuity equation or fractional conservation of mass [26]. It was shown that when fluid density can be homogenized as a power law function in space (e.g., fractal function) the Caputo fractional Taylor expansion of two terms exactly represents the density's power law relation. From a physical perspective, a power-law density relation can be motivated by fluids within a porous media [26]. This facilitates formulating an exact representation of the continuity equation by using first order fractional derivatives. This same power-law density function would otherwise require an infinite number of integer order derivatives from the Taylor expansion to obtain the same accuracy as one fractional Caputo derivative. The compactness gained by a small number of fractional derivatives must be balanced by the non-local properties of the fractional order operator which requires an integral calculation for the Caputo or Riemann-Louiville version [27]. In other works, Mainardi, Luchko and Paginini [13] have given solutions to space-time fractional order balance equations that follow a stretched exponential under certain limiting conditions in space and time. From a Bayesian perspective, the problem can be flipped around and cast as an inference of a probability density from sparse fractal data. In doing so, we illustrate how fractional order kinematic constraints lead to a stretched exponential density which contains the limiting case of a Gaussian density. It is known that a microscopic field distributed about this stretched exponential leads to the fractal space-time diffusion equation. The result highlights how collecting sparse information in space and time can be used to formulate fractal partial differential equations to identify and simulate this type of material behaviour. Importantly, such results motivate understanding the similarities and differences in local fractal derivatives versus non-local fractional derivatives for material modeling. We investigate how these characteristics inferred from Bayesian statistics are used to guide the ap-

Journal of Applied Mechanics. Received March 27, 2023;
Accepted manuscript posted April 15, 2023. doi:10.1115/1.4062389

plication of fractal or fractional order operators used in developing rate-dependent constitutive equations in elastomers.

Given the subtle but important distinctions between fractal and fractional order operators in material modeling, we evaluate assumptions that constrain elastomeric materials to follow certain trajectories that are better predicted by fractal or fractional order operators in space and time. We apply entropy dynamics [8] to better understand how our assumptions, cast as a set of constraints about polymer network displacements, provide insights on appropriate derivative operators. We illustrate how a fractional (power-law) constraint of particle displacements leads to a stretched exponential in space which, in turn, suggests a fractal derivative is also ideal to approximate deformation via a fractal deformation gradient. Time dependent properties, such as viscoelasticity, require additional assumptions on the irreversible characteristics of entropy generation. The covariance properties of particle interactions are introduced in the entropy dynamics framework to provide guidance on time dependent particle interactions. Under Gaussian approximations, the variance or covariance of particle motion is linear in time which can be accurately approximated by integer order time derivatives. If the covariance evolves over a power-law in time, we show that a fractal time derivative within the diffusion equation exactly models such behavior. We compare this relation to fractional order viscoelasticity assumptions through experimental validation on the uniaxial stress-stretch behavior of dielectric elastomers, VHB 4910 and 4949. We also offer insight on when fractal and fractional order derivatives will give the same or different material model predictions.

The entropy dynamics framework quantifies conditional probability densities of future material particle positions given their original undeformed positions. The particles are broken down into two different sets. One set of particles is defined to be observable or controllable by an external loading device in a way that particles move in an affine manner based on boundary conditions. These displacements are typically defined by transformations which map changes on a boundary to the bulk volume. The set of particles is denoted by their Eulerian or deformed position in three dimensional space as $\mathbf{x}_\alpha(t)$ for $\alpha = 1, \ldots, n$ particles in some representative volume element (Eulerian frame volume). A second set of unobservable or uncontrollable particles are denoted by $\mathbf{y}_\alpha(t)$ for $\alpha = 1, \ldots, m$ such that the total number of particles in the material is $N = n + m$. These unobservable particles contribute to heat, residual effects, damage, or other irreversibilities that cannot be controlled by an external loading device. We apply entropy dynamics to construct a model containing constraints on both the controllable $\mathbf{x}_\alpha$ and uncontrollable $\mathbf{y}_\alpha$ particle positions and their time dependent properties. These manifest through quantifying the uncertainty of a continuum homogenization of the particles as a field mapped onto the Lagrangian (undeformed) configuration that we denote by $\mathbf{X}$. This requires first quantifying a Bayesian posterior density as a joint probability of the continuum homogenized kinematics: $\mathbf{x} = \mathbf{x}(\mathbf{X}, t)$ and $\mathbf{y} = \mathbf{y}(\mathbf{X}, t)$. Once the Bayesian posterior density is quantified, this naturally leads to a maximization of the likelihood of future deformation $\mathbf{x}(\mathbf{X}, t)$ and internal state changes $\mathbf{y}(\mathbf{X}, t)$ based on thermodynamic functions that are obtained from the posterior density. The thermodynamic functions provide the information required to quantify fractal or fractional hyperelastic and viscoelastic constitutive relations. We then extend the kinematic relations to the fractal domain to accommodate complexities that follow power-law behavior in space and time.

In the following section, we first outline how we apply entropy dynamics to obtain a Bayesian posterior probability. This is followed by the introduction of conditional probability constraints on $\mathbf{x} = \mathbf{x}(\mathbf{X}, t)$ and $\mathbf{y} = \mathbf{y}(\mathbf{X}, t)$ as well as fractional constraints that lead to thermodynamic potentials and entropy generation expression that relate fractal elastomer network structure to kinematics constrained to move along fractal paths. We then numerically evaluate the model and validate it against viscoelastic elastomer data. Discussions are then given about the importance of constraints and its interpretation with respect to material structure when developing material models based on fractional order and fractal order derivatives. Conclusions are given in the final section.

2 THEORY

2.1 Preliminaries

We start by considering Shannon's relative entropy having the form

$$S[P, Q] = -\int_{\mathcal{D}} P(\mathbf{x}, \mathbf{y}|\mathbf{X}) \ln \left(\frac{P(\mathbf{x}, \mathbf{y}|\mathbf{X})}{Q(\mathbf{x}, \mathbf{y}|\mathbf{X})} \right) d\mathbf{x} d\mathbf{y} \tag{1}$$

where the unknown posterior density is $P(\mathbf{x}, \mathbf{y}|\mathbf{X})$ and the prior density is $Q(\mathbf{x}, \mathbf{y}|\mathbf{X})$. We will assume the prior density as flat or uniform with respect to $\mathbf{x}$ and $\mathbf{y}$ meaning that any location of $\mathbf{x}$ and $\mathbf{y}$ are equally possible given its original position $\mathbf{X}$. Note that the integral is over the representative material volume $\mathcal{D}$ in the deformed configuration. This means the probability densities are per Eulerian volume. In three dimensions, the domain $\mathcal{D}$ is

Journal of Applied Mechanics. Received March 27, 2023;
Accepted manuscript posted April 15, 2023. doi:10.1115/1.4062389

a volume where we use the notation $d\mathbf{x} = dx_1dx_2dx_3$ and $d\mathbf{y} = dy_1dy_2dy_3$. Also note that we define the entropy here as unitless meaning the probability densities define the probability of $\mathbf{x}$ and $\mathbf{y}$ given $\mathbf{X}$ over the volume $\mathcal{D}$. This requires special considerations such that the total material volume is $\mathcal{D} = \mathcal{D}_\mathbf{x} \cup \mathcal{D}_\mathbf{y}$ is disjoint in the pointwise sense $\mathcal{D}_\mathbf{x} \cap \mathcal{D}_\mathbf{y} = 0$.

Before describing the details of the model, we first highlight that if the Shannon entropy is maximized according to the variational problem

$$\delta S[P,Q] = \frac{\partial S}{\partial P}\delta P = 0 \tag{2}$$

it can be shown that the solution for the Bayesian posterior density P that maximizes $S[P,Q]$ is a uniform conditional probability that is inversely proportional to the volume [28, 29]. As one may expect, this is because we have assumed the prior is uniform and we have not included any constraints when maximizing $S[P,Q]$ except that P must integrate to one over all $\mathbf{x}$ and $\mathbf{y}$. Additional constraints are added to the model based on interactions between relative displacements of $\mathbf{x}$ and $\mathbf{y}$.

The constraint that we introduce in Section 2.2 is to minimize the relative positions between neighboring Lagrangian points: $\Delta\mathbf{x} = \mathbf{x}(\mathbf{X}+\Delta\mathbf{X},t) - \mathbf{X}$ and $\Delta\mathbf{y} = \mathbf{y}(\mathbf{X}+\Delta\mathbf{X},t) - \mathbf{Y}$ where we denote $\mathbf{Y}$ as the undeformed position of the unobservable deformed state $\mathbf{y}$. If a constraint based on $\Delta\mathbf{x}$ or $\Delta\mathbf{y}$ is added to Shannon's entropy, we find that maximizing the Shannon entropy tends to *broaden* the posterior of possible particle positions while a constraint on the squared magnitude of $\Delta\mathbf{x}$ or $\Delta\mathbf{y}$ *narrows* the posterior. The posterior becomes a Gaussian distribution rather than a uniform distribution and the width of the Gaussian depends on knowledge of the covariance matrix which is used to constrain the vector products, $\Delta\mathbf{x}\Delta\mathbf{x}$, $\Delta\mathbf{y}\Delta\mathbf{y}$, and $\Delta\mathbf{x}\Delta\mathbf{y}$ as described in the following section. The quantitative form of the Gaussian requires knowledge of covariance matrices that represent distributions of the self-interactions of $\Delta\mathbf{x}\Delta\mathbf{x}$ and $\Delta\mathbf{y}\Delta\mathbf{y}$ and the interactions $\Delta\mathbf{x}\Delta\mathbf{y}$. These covariance matrices may come from theoretical conjectures, sparse observations from experiments, or high fidelity simulations. Entropy dynamics provides a tool to evaluate the uncertainties in terms of estimates of the covariance matrix which may include time invariant and time varying components. This provides advantages in distinguishing reversible, path independent behavior (time independent covariance) from irreversible, hysteretic behavior (time dependent covariance). It also provides a way to connect information theory and information entropy with thermodynamic entropy and constitutive relations for non-Gaussian processes. This latter effect will be explored using fractional order constraints, as opposed to a quadratic constraint, to relate fractal structure to fractional order properties. This will impact both the reversible hyperelastic behavior and irreversible viscoelasticity.

2.2 Quadratic Constraints and neo-Hookean Behavior

To facilitate later development of the fractal and fractional order models, we first present the simpler model containing a quadratic constraint in the cost function. In this case, Shannon's entropy is combined with a quadratic constraint that limits the relative material displacements between neighboring points located at $\mathbf{X}$ and $\mathbf{X}+\Delta\mathbf{X}$. We start by defining the integer order Taylor expansion of the position vector of each material point that will be used in the cost function constraint. The neighboring continuum displacements are described by

$$\begin{aligned}\mathbf{x}(\mathbf{X}+\Delta\mathbf{X}) &= \mathbf{X} + \tfrac{\partial\mathbf{x}}{\partial\mathbf{X}}\cdot\Delta\mathbf{X} + \cdots,\\ \mathbf{y}(\mathbf{X}+\Delta\mathbf{X}) &= \mathbf{Y} + \tfrac{\partial\mathbf{y}}{\partial\mathbf{X}}\cdot\Delta\mathbf{X} + \cdots.\end{aligned} \tag{3}$$

We will penalize the relative positions for the observable and unobservable displacement fields. The notation $\Delta\mathbf{x} = \mathbf{x}(\mathbf{X}+\Delta\mathbf{X}) - \mathbf{X}$ is used for brevity and similarly for the uncontrollable terms as $\Delta\mathbf{y} = \mathbf{y}(\mathbf{X}+\Delta\mathbf{X}) - \mathbf{Y}$.

A quadratic constraint is used to create a cost function that balances maximizing entropy with penalties of large relative displacements. This uses the tensor product $\Delta\mathbf{x}\Delta\mathbf{x}$, $\Delta\mathbf{x}\Delta\mathbf{y}$ and $\Delta\mathbf{y}\Delta\mathbf{y}$ that are constrained to different covariance matrices associated with the relative displacement vectors and their coupling. The cost function is given by

$$\begin{aligned}H[P,Q] = S[P,Q] &- \gamma\left(\int_\mathcal{D} P(\mathbf{x},\mathbf{y}|\mathbf{X})d\mathbf{x}d\mathbf{y} - 1\right)\\ &- \mathrm{Tr}\left\{\mathbf{\Lambda}_{xx}\cdot\left(\int_\mathcal{D} P(\mathbf{x},\mathbf{y}|\mathbf{X})(\Delta\mathbf{x}\Delta\mathbf{x})d\mathbf{x}d\mathbf{y} - \mathbf{\Sigma}_{xx}\right)\right\}\\ &- \mathrm{Tr}\left\{\mathbf{\Lambda}_{xy}\cdot\left(\int_\mathcal{D} P(\mathbf{x},\mathbf{y}|\mathbf{X})(\Delta\mathbf{x}\Delta\mathbf{y})d\mathbf{x}d\mathbf{y} - \mathbf{\Sigma}_{xy}\right)\right\}\\ &- \mathrm{Tr}\left\{\mathbf{\Lambda}_{yy}\cdot\left(\int_\mathcal{D} P(\mathbf{x},\mathbf{y}|\mathbf{X})(\Delta\mathbf{y}\Delta\mathbf{y})d\mathbf{x}d\mathbf{y} - \mathbf{\Sigma}_{yy}\right)\right\}\end{aligned} \tag{4}$$

where the Lagrange multipliers include γ, $\mathbf{\Lambda}_{xx}$, $\mathbf{\Lambda}_{xy}$ and $\mathbf{\Lambda}_{yy}$. The Shannon relative entropy $S[P,Q]$ is from (1)

Journal of Applied Mechanics. Received March 27, 2023;
Accepted manuscript posted April 15, 2023. doi:10.1115/1.4062389

and there is a set of covariance matrices $\mathbf{\Sigma}_{xx}$, $\mathbf{\Sigma}_{xy}$ and $\mathbf{\Sigma}_{yy}$ (each is 3×3) which describe the distribution of the observable ($\mathbf{\Sigma}_{xx}$) and unobservable ($\mathbf{\Sigma}_{yy}$) material motion and their interactions ($\mathbf{\Sigma}_{xy}$). These covariance matrices may vary spatially and temporally. We have also used Tr to represent the trace. The quadratic constraint leads to a Gaussian density of particle displacements fluctuations.

We briefly illustrate how this Gaussian density leads to a neo-Hookean, viscoelastic constitutive model to highlight how constraints are used within the information theoretic approach. Importantly, our selection of the quadratic constraint restricts the posterior density to material displacements that are distributed about a Gaussian density. This neglects the possibility of nonlinear effects that may manifest as extreme events such as internal displacements during unraveling of polymer entanglement and random walks along a fractal polymer network which are later described in Section 3.1.

We take the Gaussian probability obtained from maximizing (4) to construct a entropy function that we use to develop the rate dependent, stress-stretch constitutive relations. We neglect internal energy (u) changes within an elastomer and treat the Helmholtz energy density as $\psi = u - Ts_T \approx -Ts_T$ where T is temperature and s_T is the thermodynamic entropy density. We conduct the analysis in the limit of infinitesimal relative displacements $\Delta\mathbf{X} \to d\mathbf{X}$ from (3) such that we have the conventional deformation gradient as the internal state. This is described by $d\mathbf{x} \simeq \mathbf{F} \cdot d\mathbf{X}$ where we neglect higher order terms in (3) and we have defined the deformation gradient as $\mathbf{F} = \frac{\partial \mathbf{x}}{\partial \mathbf{X}}$. We also include the deformation gradient associated with the unobservable internal states as $\mathbf{\Gamma} = \frac{\partial \mathbf{y}}{\partial \mathbf{X}}$. The key relations associated with predicting material motion of the observable and unobservable displacement fields are denoted by

$$d\mathbf{x} = \mathbf{F} \cdot d\mathbf{X} \qquad \text{and} \qquad d\mathbf{y} = \mathbf{\Gamma} \cdot d\mathbf{X} \tag{5}$$

$$\widetilde{\mathbf{F}} = \begin{bmatrix} \mathbf{F} & \mathbf{0} \\ \mathbf{0} & \mathbf{\Gamma} \end{bmatrix} \qquad \text{and} \qquad \mathbf{\Sigma} = \begin{bmatrix} \mathbf{\Sigma_{xx}} & \mathbf{\Sigma_{xy}} \\ \mathbf{\Sigma_{yx}} & \mathbf{\Sigma_{yy}} \end{bmatrix} \tag{6}$$

We substitute these deformation gradients into the posterior probability density that maximizes (4). For brevity, we let $C_\Sigma = \frac{1}{\sqrt{(2\pi)^D |\mathbf{\Sigma}|}}$, where the covariance matrix $\mathbf{\Sigma}$ is defined in (6), $D = 6$, and then the probability is

$$P(\mathbf{x}, \mathbf{y}|\mathbf{X}) = C_\Sigma e^{-\frac{1}{2} d\mathbf{X} \cdot \widetilde{\mathbf{F}}^T \cdot \mathbf{\Sigma}^{-1} \cdot \widetilde{\mathbf{F}} \cdot d\mathbf{X}}. \tag{7}$$

To define the thermodynamic entropy, we apply a different measure than directly using the Shannon entropy. A rigorous comparison between two different entropy functions (Gibbs H_G and Boltzmann H_B) has been discussed elsewhere [30]. These two entropy functions differ in the following way. The Gibbs energy function accommodates interactions among neighboring particles while the Boltzmann version neglects particle correlation (e.g., ideal gas). The Gibbs entropy function is equivalent to Shannon's entropy (excluding the prior). Upon further analysis given by Jaynes [30], the thermodynamic entropy can be described more simply by $S = k \ln(P)$ where k is Boltzmann's constant. The Boltzmann entropy neglects explicit material correlations and measures the phase volume of "reasonably probable" events. Since our probability is defined over the continuum of particle motion by $\mathbf{x} = \mathbf{x}(\mathbf{X}, t)$, we directly use the posterior density of particle kinematics to define the thermodynamic entropy using Boltzmann's form of entropy

$$S_T = k \ln [P(\mathbf{x}, \mathbf{y}|\mathbf{X})]. \tag{8}$$

This estimate of the thermodynamic entropy S_T is the total entropy of a volume V of interest. The thermodynamic entropy density must be normalized by an appropriate representative volume which we denote by Ω_0 in the undeformed (Lagrangian) volume such that $s_T = S_T/\Omega_0$. This form of the thermodynamic entropy density is used to formulate the rate dependent stress-stretch constitutive relations.

To illustrate, we evaluate the characteristics of an ideal Gaussian polymer network given the Gaussian posterior that was obtained from the tensor product constraint in the cost function. Simplifications are made by assuming all material points are observable meaning all material points are distributed about Gaussian density and remain Gaussian for all deformation states considered. This means $\mathbf{y}$ can be neglected and $\mathbf{\Sigma}_{xy}$ and $\mathbf{\Sigma}_{yy}$ are irrelevant. We note that the assumption of Gaussian behavior is applicable to all future material displacements relative to the undeformed state. This is inherent in the fixed constraint $\mathbf{\Sigma}_{xx}$ within (4). It is well known that the Gaussian network neglects significantly large deformation and is only applicable for stretch ratios before strain hardening occurs [24, 3]. This limitation is addressed in the subsequent section.

Journal of Applied Mechanics. Received March 27, 2023;
Accepted manuscript posted April 15, 2023. doi:10.1115/1.4062389

The thermodynamic entropy based on (7) gives

$$s_T = \frac{k}{\Omega_0}\left(\ln C_\Sigma - \frac{1}{2}\left(d\mathbf{X}\cdot\mathbf{F}^T\cdot\boldsymbol{\Sigma}_{xx}^{-1}\cdot\mathbf{F}\cdot d\mathbf{X}\right)\right). \tag{9}$$

We make a further assumption that all particles move independently (zero covariance) and their variance in displacement is equal and homogeneous such that $\boldsymbol{\Sigma}_{xx} = \sigma_0^2\mathbf{I}$ where σ_0^2 is the variance and $\mathbf{I}$ is the identity matrix. Under these assumptions, the deformation gradient and their relative particle distances prior to deformation are defined to be equivalent for the entire volume Ω_0 which gives

$$s_T = \frac{k}{\Omega_0}\left(\ln C_\Sigma - \frac{1}{2\sigma_0^2}\left(d\mathbf{X}\cdot\mathbf{F}^T\cdot\mathbf{F}\cdot d\mathbf{X}\right)\right). \tag{10}$$

The Helmholtz free energy density is then

$$\psi = -\frac{kT}{\Omega_0}\left(\ln C_\Sigma - \frac{1}{2\sigma_0^2}\left(d\mathbf{X}\cdot\mathbf{F}^T\cdot\mathbf{F}\cdot d\mathbf{X}\right)\right). \tag{11}$$

As expected, this shares characteristics with the classic neo-Hookean hyperelastic model that describes finite deformation of polymers within the regime of Gaussian network distributions. Note that in this free energy function, $d\mathbf{X}$, is a set of constants and ψ then depends quadratically on the deformation gradient.

In the next section, we will change the tensor constraint from a quadratic to a fractional constraint to accommodate fat-tail probability distributions of particle displacements often exhibited by fractal structures. We will also introduce rate-dependent effects governing viscoelasticity. This provides a means to correlate non-Gaussian polymer network configurations with complex constitutive relations where rate dependent polymer deformation may follow fractal space-time complexities.

3 FRACTAL AND FRACTIONAL ORDER MODEL

3.1 Fractional Constraints and Non-Gaussian Hyperelasticity

Large elastomer deformation can lead to non-Gaussian polymer network distributions where softening followed by hardening in the stress-stretch behavior may be observed as the underlying polymer network deforms significantly. In this section, we extend the information theoretic framework that resulted in a neo-Hookean free energy in Section 2.2 to fractional order deformation constraints to accommodate nonlinear stress-stretch behavior often observed during large elastomer deformation.

We previously described motion of particles over a Euclidean domain in terms of the integer Taylor expansion in (3). We argue in this section that a fractal measure of material displacement is a better predictor of materials exhibiting this form of complexity. This complexity originates in the form of multiscale material structure that is not perfectly crystalline nor perfectly random. The goal is to predict the future configurations of such fractal structure upon irreversible mechanical loading. We propose to use a fractal metric for the material configuration and fractal derivative operators to predict future configurations after applying mechanical loading. The choice of fractal derivatives over fractional derivatives is discussed later in Section 3.2. We represent the deformation on a fractal domain using

$$\boldsymbol{\mu}(\mathbf{x}+\Delta\mathbf{x},t) \simeq \boldsymbol{\mu}(\mathbf{x},t) + \frac{\partial\boldsymbol{\mu}}{\partial\mathbf{x}^\beta}\cdot\Delta\mathbf{x}^\beta \tag{12}$$

where the fractal vector of deformed material points is $\boldsymbol{\mu} = \boldsymbol{\mu}(\mathbf{x},t)$ as a function of the Eulerian frame coordinates, and $\beta > 0$ is the order of fractal derivative. Given the assumption of fractal material structure which may produce polymer network displacements that are fractal or multi-fractal (i.e, random fractals), we use a displacement measure in the fractal domain that is defined by $\boldsymbol{\mu} = \boldsymbol{\mu}(\mathbf{x}(\mathbf{X},t),t)$. This fractal metric is related to the Euclidean domain based on a power-law relation often described by a density of state [15, 22]. We focus on isotropic densities of state and fractal exponents in this analysis; more details are given by Tarasov [27]. To simplify the notation, we include observable ($\boldsymbol{\mu}^{(x)}$) and unobservable ($\boldsymbol{\mu}^{(y)}$) fractal measures as a single vector field $\boldsymbol{\mu} = [\boldsymbol{\mu}^{(x)}, \boldsymbol{\mu}^{(y)}]$ which are analogous to the Euclidean model from Section 2. The relationship between the fractal measure in each coordinate direction ($\mu_i^{(x,y)}$) and the normalized Cartesian (Eulerian) direction $\overline{x}_i$ for $i = 1,2,3$ is defined to be

$$\begin{aligned}\mu_i^{(x)} &= \tfrac{\pi^{\nu/2}}{2^\nu\Gamma(\nu/2+1)}|\overline{x}_i|^\nu,\\ \mu_i^{(y)} &= \tfrac{\pi^{\nu/2}}{2^\nu\Gamma(\nu/2+1)}|\overline{y}_i|^\nu\end{aligned} \tag{13}$$

where $\overline{x}_i = \frac{x_i}{l_0}$ and $\overline{y}_i = \frac{y_i}{l_0}$ are normalized coordinates given the characteristic length scale l_0 in the Eulerian

Journal of Applied Mechanics. Received March 27, 2023;
Accepted manuscript posted April 15, 2023. doi:10.1115/1.4062389

frame and $\Gamma()$ is the gamma function not to be confused with the tensor in (5) [31]. The power-law scaling is denoted by ν.

To establish translational and rotational invariance, we restrict the radius of some sphere to a finite set that we define by the characteristic length l_0 which is used to define a representative continuum volume element of sufficient size to represent the fractal structure. If we assume that $\beta = \nu$ from (12), this relation becomes

$$\begin{aligned} d\mu_i^{(x)} &= \frac{\pi^{\nu/2}}{2^{\nu-1} l_0 \Gamma(\nu/2)} F_{iK} dX_K, \\ d\mu_i^{(y)} &= \frac{\pi^{\nu/2}}{2^{\nu-1} l_0 \Gamma(\nu/2)} \Gamma_{iK} dX_K \end{aligned} \tag{14}$$

such that the fractal deformation gradient scales with the Euclidean deformation gradient according to $F_{iK}^{\nu} = \frac{\pi^{\nu/2}}{2^{\nu-1} l_0 \Gamma(\nu/2)} F_{iK}$ where, $F_{iK} = \frac{\partial x_i}{dX_K}$ for $K = 1, 2, 3$. Similar scaling applies to the deformation gradient associated with the unobservable internal states $\Gamma_{iK} = \frac{\partial y_i}{\partial X_K}$. A more detailed discussion on this invariance is available [31].

The cost function that constrains fractal displacements to a fractional order constraint is proposed to be

$$\begin{aligned} H[P,Q] = S[P,Q] - \gamma \left(\int_{\mathcal{D}} P(\boldsymbol{\mu}|\mathbf{X}) d\boldsymbol{\mu} - 1 \right) \\ - \mathrm{Tr} \left\{ \boldsymbol{\Lambda} \cdot \left(\int_{\mathcal{D}} P(\boldsymbol{\mu}|\mathbf{X}) \mathbf{C_X}^{\frac{\nu}{2}} d\boldsymbol{\mu} - \boldsymbol{\Sigma}^{\frac{\nu}{2}} \right) \right\} \end{aligned} \tag{15}$$

where the fractional order covariance matrix is $\boldsymbol{\Sigma}$ is given in (6) and the corresponding 6×6 Lagrange multiplier matrix is $\boldsymbol{\Lambda}$ and $\mathbf{C_X}^{\nu/2} = (d\boldsymbol{\mu} d\boldsymbol{\mu})^{\nu/2}$. These second order tensors are raised to a power using conventional operations by rotating the tensors to their eigendirections, applying the exponents to the eigenvalues, and rotating the tensors back to their original directions [1]. Moreover, these measures are positive semi-definite, symmetric and therefore are real-valued matrices. The fractional power law exponent ν penalizes fractal displacements relative to their initial positions. It is expected that this exponent is related to the original fractal structure, however, the exact relationship between the fractal dimension of a polymer network and the fractional parameter ν is non-trivial [1, 32].

The general form of the cost function in the eigendirection is given by

$$\begin{aligned} H[P,Q] = S[P,Q] - \gamma \left(\int_{\mathcal{D}} P(\hat{\boldsymbol{\mu}}|\mathbf{X}) d\hat{\boldsymbol{\mu}} - 1 \right) \\ - \mathrm{Tr} \left\{ \hat{\boldsymbol{\Lambda}} \cdot \left(\int_{\mathcal{D}} P(\hat{\boldsymbol{\mu}}|\mathbf{X}) \mathbf{D}^{\frac{\nu}{2}} d\hat{\boldsymbol{\mu}} - \hat{\boldsymbol{\Sigma}}^{\frac{\nu}{2}} \right) \right\}. \end{aligned} \tag{16}$$

where $\hat{\boldsymbol{\Lambda}}$ is rotated Lagrange multiplier matrix and it is assumed that $\mathbf{C_X}$ has the same eigendirections as $\boldsymbol{\Lambda}$. The matrix $\mathbf{D}$ is diagonalized matrix with eigenvalues as diagonal entries of $\mathbf{C_X}$.

Optimizing H with respect to P we get

$$-\ln(Q) + \ln(P) + 1 + \gamma + Tr\left(\hat{\boldsymbol{\Lambda}} \cdot \mathbf{D}^{\nu/2}\right) = 0, \tag{17}$$

The posterior density is

$$P(\hat{\boldsymbol{\mu}}|\mathbf{X}) = Q e^{-(1+\gamma+Tr(\hat{\boldsymbol{\Lambda}} \cdot \mathbf{D}^{\nu/2})}. \tag{18}$$

The Lagrange multiplier γ is re-written in terms of a partition function Z using the normalization constraint on the probability density according to

$$Z = \int_{\mathcal{D}} e^{-(Tr(\hat{\boldsymbol{\Lambda}} \cdot \mathbf{D}^{\nu/2}))} d\hat{\boldsymbol{\mu}} = Q^{-1} e^{1+\gamma} \tag{19}$$

such that the posterior density is

$$P(\hat{\boldsymbol{\mu}}|\mathbf{X}) = Z^{-1} e^{-(Tr(\hat{\boldsymbol{\Lambda}} \cdot \mathbf{D}^{\nu/2}))}. \tag{20}$$

We solve for Z and $\hat{\boldsymbol{\Lambda}}$ using the constraints and symmetry of P about $|d\hat{\boldsymbol{\mu}}| = 0$. Assuming Q is a flat prior, after solving we get

$$Z^{-1} = \frac{\nu^6}{2^6 (\Gamma(\nu^{-1}))^6} \left(\prod_{i=1}^{6} \hat{\Lambda}_{ii} \right)^{\frac{1}{\nu}} \tag{21}$$

where $\Gamma(\nu^{-1})$ is again the gamma function.

The final form of the posterior P is

$$P(\boldsymbol{\mu}|\mathbf{X}) = C_\nu e^{-\left(\frac{\Gamma(\frac{\nu+1}{\nu})}{\Gamma(\nu^{-1})} Tr(\boldsymbol{\Sigma}^{-\nu/2} \cdot C_{\mathbf{x}}{}^{\nu/2}) \right)} \tag{22}$$

Journal of Applied Mechanics. Received March 27, 2023;
Accepted manuscript posted April 15, 2023. doi:10.1115/1.4062389

where $C_\nu = \frac{\nu^6}{2^6(\Gamma(\nu^{-1}))^6}\left(\frac{\Gamma(\frac{\nu+1}{\nu})}{\Gamma(\nu^{-1})}\right)^{\frac{6}{\nu}}(\det(\mathbf{\Sigma}^{-\frac{\nu}{2}}))^{\frac{1}{\nu}}$.

Note that for $\nu = 2$, substituting (14) into the above density and using (6) leads to $\frac{1}{\sqrt{(2\pi)^6\det(\mathbf{\Sigma})}}\exp\left(-\frac{1}{2}d\mathbf{X}\cdot(\widetilde{\mathbf{F}}^\beta)^T\cdot\mathbf{\Sigma}^{-1}\cdot\widetilde{\mathbf{F}}^\beta\cdot d\mathbf{X}\right)$ which coincides with 6-dimensional multivariate Gaussian distribution as expected.

Following the same derivation from Section 2.2, a Helmholtz free energy expression can be obtained from the posterior in (11) which is given here by

$$\psi_\nu = -\frac{kT}{\Omega_0}\left(\ln C_\nu - \left(\frac{\Gamma(\frac{\nu+1}{\nu})}{\Gamma(\nu^{-1})}Tr\left(\mathbf{\Sigma}^{-\nu/2}\cdot {C_\mathbf{x}}^{\nu/2}\right)\right)\right). \tag{23}$$

Based on (23), the Helmholtz free energy is defined as a function of the fractal deformation gradient, $\psi_\nu = \psi_\nu(\mathbf{F}^\beta)$ which can be re-written in terms of the principal stretches that we define as λ_L^β for the principal directions $L = 1, 2, 3$. Furthermore, we denote the observable stretch as $\lambda_L^{\beta,x}$ and unobservable stretch as $\lambda_L^{\beta,y}$. Following the procedure that gives (14), a scalar factor relates the fractal stretch to the observable deformation gradient according to

$$\lambda_L^{\beta,x} = \frac{\pi^{\beta/2}}{2^{\beta-1}l_0\Gamma(\beta/2)}\lambda_L \tag{24}$$

where l_0 is the characteristic length scale and Γ is the gamma function. An analogous relationship exists for $\lambda_L^{\beta,y}$. In the case where $\beta = 1$ and $l_0 = 1$, the fractal stretch equals the measurable stretch.

We introduce viscoelasticity into this model by adjusting the constraints for particle motion as given by the last term in (16). This constraint on relative particle motion ($d\boldsymbol{\mu}$) is divided into observable ($d\boldsymbol{\mu}^{(x)}$) and unobservable ($d\boldsymbol{\mu}^{(y)}$) terms that are independent. The unobservable relative displacements contribute to the viscoelastic effect described in the following section. This gives three separate constraints in the cost function with a fractional variance on the observable ($\mathbf{\Sigma}_{xx}^{\frac{\nu}{2}}$), unobservable ($\mathbf{\Sigma}_{yy}^{\frac{\nu}{2}}$), and their interactions ($\mathbf{\Sigma}_{xy}^{\frac{\nu}{2}}$) fractal relative displacements.

These constraints result in the following Helmholtz free energy function

$$\psi_\nu = T\left[f_0^{11}(\lambda_L^{\beta,x}\lambda_L^{\beta,x})^{\nu/2} + 2f_0^{12}(\lambda_L^{\beta,x}\lambda_L^{\beta,y})^{\nu/2} + f_0^{22}(\lambda_L^{\beta,y}\lambda_L^{\beta,y})^{\nu/2}\right] \tag{25}$$

where T is temperature, the principle directions are $L = 1, 2, 3$, and the constitutive parameters include one governing observable stretch f_0^{11}, one governing non-observable stretch f_0^{12}, and one coupling term f_0^{22}. These parameters consist of the gamma function and time invariant portion of the covariance matrix given in (23); see [31] for details.

3.2 Fractal and Fractional Order Operators

This section re-visits the integer Taylor series of a function and then compares it to the fractal Taylor and fractional series expansions space. To simplify the analysis, we illustrate its effect in terms of a general scalar function $f(x)$. Its use is given here to demonstrate the utility of fractal derivatives in space and time for systems that follow power-law (fractal relationships). This has implications on predicting the kinematics of elastomers upon mechanical loading.

The Taylor expansion of a smooth, infinitely differentiable, function f at $x = x_0$ is the power series given by

$$f(x) = f(x_0) + f'(x_0)(x-x_0) + \frac{f''(x_0)}{2}(x-x_0)^2 + ... = \sum_{n=0}^{\infty}\frac{f^{(n)}(x_0)}{n!}(x-x_0)^n \tag{26}$$

where $f^{(n)}(x_0)$ is the n-th derivative of f evaluated at $x = x_0$.

It is clear that the first two terms of the series provide a linear approximation of the function around $x = x_0$. For nonlinear functions, extrapolation in space and time limits accuracy, dependent upon the magnitude of the nonlinearity.

3.2.1 *Fractal derivative*

The fractal derivative of order $\beta > 0$ of a function f is defined by

$$\frac{d}{dx^\beta}f(x) = \lim_{x_0\to x}\frac{f(x_0)-f(x)}{{x_0}^\beta - x^\beta} \tag{27}$$

Journal of Applied Mechanics. Received March 27, 2023;
Accepted manuscript posted April 15, 2023. doi:10.1115/1.4062389

The fractal derivative is related to the ordinary derivative in the following manner.

$$\begin{aligned}\frac{d}{dx^\beta}f(x) &= \lim_{x_0\to x}\frac{f(x_0)-f(x)}{{x_0}^\beta - x^\beta}\\ &= \lim_{x_0\to x}\frac{f(x_0)-f(x)}{x_0-x}\cdot\frac{x_0-x}{{x_0}^\beta - x^\beta}\\ &= \frac{df(x)}{dx}\cdot\frac{d}{dx^\beta}(x_0-x)\\ &= \frac{x^{1-\beta}}{\beta}\frac{df(x)}{dx}\end{aligned} \tag{28}$$

Using the definition of the fractal derivative in (27), one can construct the fractal Taylor series expansion. One of the significant differences between the fractal Taylor expansion and integer-order Taylor expansion is that the approximation basis consists of powers of x^β unlike the integer order, which uses polynomials as the basis functions. Thus, the goal is to approximate functions with $({x^\beta - {x_0}^\beta})^n$ instead of $(x-x_0)^n$ as done in (26). Deriving the right expansion coefficient b_k completes the fractal Taylor series of f around $x = x_0$

$$\begin{aligned}f(x) &= b_0 + b_1(x^\beta - {x_0}^\beta) + b_2({x^\beta - {x_0}^\beta})^2 + ...\\ &= \sum_{k=0}^{\infty} b_k({x^\beta - {x_0}^\beta})^k\end{aligned} \tag{29}$$

where $b_0 = f(x_0)$.

The coefficients b_k are obtained using a similar procedure to finding the coefficients for the integer Taylor series. As one can infer from the relation between the regular derivative and fractal derivative (28), the expansion coefficients b_k have a similar form to integer Taylor coefficients. These relations are

$$b_k = \frac{1}{k!}\left(\frac{d}{dx^\beta}\right)^k f(x = x_0) \tag{30}$$

where $(\frac{d}{dx^\beta})^k f$ is the k-th fractal derivative of function f of order β.

We are particularly interested in fractal derivatives for a given material with an initial fractal structure and the possibility of displacements that follow fractal paths of motion in space and time. Since fractals follow a power-law, accurate approximation of power-law type functions may improve predictions. The fractal Taylor series is an excellent estimator of power-law functions. The first two terms of the fractal Taylor series are exact for power-law functions as long as we choose the proper fractal order. For example, consider a power-law function $f(x) = x^\alpha$ for some $\alpha \in \mathbb{R}$. Then the first two term approximate of this function around $x = x_0$, using a fractal Taylor series of fractal order β, is

$$\begin{aligned}f(x) &\approx f(x_0) + \frac{d}{dx^\beta}f(x_0)(x^\beta - x_0^\beta)\\ &= x_0^\alpha + \frac{x^{1-\beta}}{\beta}\frac{dx^\alpha}{dx}(x^\beta - x_0^\beta)\\ &= x_0^\alpha + \frac{\alpha x^{1-\beta}}{\beta}x^{\alpha-1}(x^\beta - x_0^\beta)\\ &= x_0^\alpha + \frac{\alpha}{\beta}x^{\alpha-\beta}(x^\beta - x_0^\beta)\end{aligned} \tag{31}$$

If $\alpha = \beta$, then we recover the original function $f(x) = x^\alpha$. From the above calculations, it is clear that for power functions, the two-term fractal Taylor expansion is exact regardless of the point about which the Taylor expansion is carried out. This behavior is lacking in the fractional Taylor series, which we discuss below.

3.2.2 *Fractional Caputo Derivative*

The general definition for the Caputo fractional derivative, D_x^α, is given by

$$D_x^\alpha f(x) = \frac{1}{\Gamma(n-\alpha)}\int_0^x \frac{f^{(n)}(s)}{(x-s)^{\alpha+1-n}}ds \tag{32}$$

$$\text{for } n-1 < \alpha \le n,\ n \in \mathbb{N}$$

where $\alpha > 0$ is the fractional order of the derivative and n is the smallest integer greater than α. The gamma function is given by $\Gamma(n-\alpha)$ and $f^{(n)}(s)$ represent the n^{th} integer derivative evaluated at point s. The fractional Taylor expansion based on fractional Caputo derivatives has been constructed and studied elsewhere [33]. The Caputo fractional Taylor expansion has the form

$$\begin{aligned}f(x) = f(x_0) &+ D_x^\alpha f(z+)\frac{(x-x_0)^\alpha}{\Gamma(\alpha+1)}\\ &+ D_x^\alpha D_x^\alpha f(z+)\frac{(x-x_0)^{2\alpha}}{\Gamma(2\alpha+1)} + ...,\end{aligned} \tag{33}$$

Journal of Applied Mechanics. Received March 27, 2023;
Accepted manuscript posted April 15, 2023. doi:10.1115/1.4062389

where $f(x+)$ represents the right hand limit of f at x. For functions following power law of the form $f(x) = q + (x - x_0)^p$ for some $p > 0$, Caputo based fractional two-term Taylor approximation is exact. [26]

One significant difference between the fractal Taylor series and Caputo based fractional Taylor series is their basis of expansions. As mentioned earlier, fractal series relies on $(x^\alpha - {x_0}^\alpha)$ type of basis while the fractional series uses $(x - x_0)^\alpha$. This difference in basis results in a slightly different approximation of functions. More importantly, depending on the functions being approximated, one method can outperform the other as shown in Figure 1. For example, two-term fractional Taylor series is exact for $f(x) = q + (x - x_0)^p$ but not for $g(x) = q + x^p - {x_0}^p$ (again $p > 0$) while the opposite holds true for the fractal two-term Taylor expansion. This difference in basis and approximation is explored by applying both operators in time domain to model viscoelasticity.

3.3 Fractal Viscoelasticity

The stretched exponential posterior given by (22) contains a covariance matrix that is assumed to be time dependent. This time dependence accommodates non-conservative behavior which in the case of elastomers is a consequence of heat generation and elastomer network configurational losses within the polymer network. In the limiting case of time invariance, the posterior density and subsequent forms of Gibbs and Boltzmann entropy results in a reversible hyperelastic-like function. We delineate the reversible and irreversible components of the total entropy according to the observable and unobservable internal state variables to model viscoelasticity. This distinguishes different components of the total Boltzmann entropy function given by

$$s_T = \frac{k}{\Omega_0} \ln\left(P(\boldsymbol{\mu}|\mathbf{X})\right) \tag{34}$$

where $P(\boldsymbol{\mu}|\mathbf{X})$ was previously given by (22) to have time dependence within the covariance matrix and Ω is the Lagrangian volume element.

The time-varying characteristics within the posterior are associated with the unobservable relative displacements which we estimate using the deformation gradient of the internal state $\boldsymbol{\Gamma}^\beta$. By expanding terms within the total entropy, we obtain a superposition of reversible and irreversible entropy components. The explicit form of this entropy is

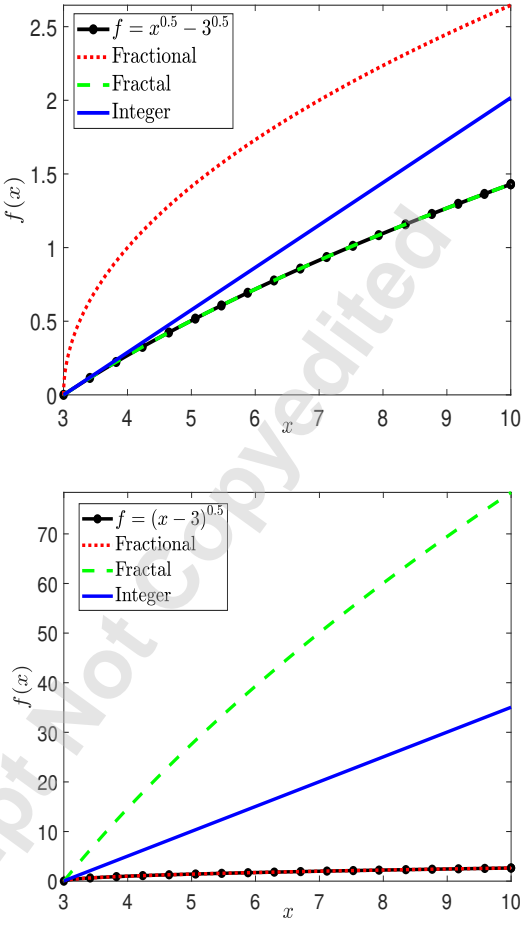

Fig. 1: Fractal, fractional and integer order two-term Taylor series approximations of two different basis functions.

$$s_T = \frac{k}{\Omega_0}\left\{\left(\mathbf{F}^\beta \cdot \boldsymbol{\Sigma}_{xx}^{-\nu/2} \cdot \mathbf{F}^\beta\right)^{\nu/2} + \left(\mathbf{F}^\beta \cdot \boldsymbol{\Sigma}_{xy}^{-\nu/2} \cdot \boldsymbol{\Gamma}^\beta\right)^{\nu/2} + \left(\boldsymbol{\Gamma}^\beta \cdot \boldsymbol{\Sigma}_{yy}(t)^{-\nu/2} \cdot \boldsymbol{\Gamma}^\beta\right)^{\nu/2}\right\}. \tag{35}$$

where we assume explicit time dependence in $\boldsymbol{\Sigma}_{yy}(t)$.

The entropy generation is taken to be the terms in (35) which contain the internal state $\boldsymbol{\Gamma}^\beta$. We explicitly define it as

$$s_g = \frac{k}{\Omega_0}\left\{\left(\mathbf{F}^\beta \cdot \boldsymbol{\Sigma}_{xy}^{-\nu/2} \cdot \boldsymbol{\Gamma}^\beta\right)^{\nu/2} + \left(\boldsymbol{\Gamma}^\beta \cdot \boldsymbol{\Sigma}_{yy}(t)^{-\nu/2} \cdot \boldsymbol{\Gamma}^\beta\right)^{\nu/2}\right\}. \tag{36}$$

To satisfy the second law of thermodynamics, the

time rate of change of s_g must be positive semi-definite, therefore, we restrict

$$\frac{ds_g}{dt^\alpha} = \frac{\partial s_g}{\partial \Gamma^\beta_{iK}} \frac{\partial \Gamma^\beta_{iK}}{\partial t^\alpha} = F(\dot{\Gamma}^{(\alpha)}_{iK}) \geq 0 \tag{37}$$

where $F(\dot{\Gamma}^{(\alpha)}_{iK})$ is an unknown function that depends on the fractal time rate of change of the internal state. We have also taken the *fractal* time rate of change of the entropy generation with order $0 < \alpha \leq 1$ as denoted by $\dot{\Gamma}^{(\alpha)}_{iK}$. This is motivated by the previous discussion of fractal Taylor series approximations of power law functions. In the case of entropy generation, we assume a power-law dependence in time which is governed by the time-varying properties in the covariance matrix $\mathbf{\Sigma}_{yy}(t)$. We assume this covariance matrix increases in time according to the power-law dependence, t^α. We also simplify the analysis by assuming the covariance is isotropic. In this case we let, $\mathbf{\Sigma}_{yy} = \Sigma_0(t) = \Sigma_0 \mathbf{I}(t^\alpha - t_0^\alpha)$ where Σ_0 is a positive constant and t_0 is the initial time. The order of the time derivative α is unknown but related to the fractal structure constraint ν. We infer both ν and α from experiments as detailed in Section 4.

The simplest function that ensures $F(\dot{\Gamma}^{(\alpha)}_{iK})$ is positive definite is

$$F(\dot{\Gamma}^{(\alpha)}_{iK}) = \eta \dot{\Gamma}^{(\alpha)}_{iK} \dot{\Gamma}^{(\alpha)}_{iK}. \tag{38}$$

where η is an unknown viscous term. A comparison of (37) and (38) gives us the viscoelastic relation necessary to solve for Γ_{iK} which is

$$\eta \dot{\Gamma}^{(\alpha)}_{iK} = \frac{\partial s_g}{\partial \Gamma_{iK}} = Q_{iK} \tag{39}$$

where we have denoted the fractal viscoelastic stress by Q_{iK} in terms of the change in entropy generation with respect to the internal state Γ_{iK}.

Our assumption of the fractal time derivative model has assumed that the covariance matrix governing the internal state increases in time proportional to a special power law function. In the limiting case, $\alpha = 1$, we obtain the classical diffusion process that follows a Gaussian density. We have generalized this to power law relations with the limiting case of a Gaussian density when the time order is $\alpha = 1$ and the spatial order is $\nu = 2$. We give additional support for using a fractal time derivative by starting with a stretched exponential probability density in space and time. It is shown that when the internal state $\boldsymbol{\mu}$ is homogenized over a stretched exponential, fractal time derivatives in space and time lead to the fractal diffusion equation. This extends results illustrated by Falconer[34] for the limiting case of a Gaussian distribution.

To illustrate this relation, we write the homogenized fractal displacements as

$$\boldsymbol{\mu}(\mathbf{X}', t+h) = C_\nu \int_\Omega G \cdot \boldsymbol{\mu}(\mathbf{X}, h) dX_1 dX_2 dX_3 \tag{40}$$

where

$$G = \exp\left[\frac{-\Gamma\left(\frac{\nu+1}{\nu}\right) |\boldsymbol{\mu}(\mathbf{X}', t) - \boldsymbol{\mu}(\mathbf{X}, t)|^\nu}{\Gamma(\nu^{-1}) \Sigma_0^{\frac{\nu}{2}} t^\alpha} \right] \tag{41}$$

and the fractal displacement is homogenized over all neighboring Lagrangian points $\mathbf{X}$ relative to $\mathbf{X}'$ where $\mathbf{X}' = \mathbf{X} + \mathbf{dX}$. We have also explicitly re-written (12) in the reference configuration as $d\boldsymbol{\mu} = \boldsymbol{\mu}(\mathbf{X} + \mathbf{dX}, t) - \boldsymbol{\mu}(\mathbf{X}, t)$.

Using the definition of the fractal derivatives in space and time as

$$\begin{aligned} \frac{\partial \mu_i}{\partial t^\zeta} &= \frac{1}{\zeta t^{\zeta-1}} \frac{\partial \mu_i}{\partial t} \\ \frac{\partial \mu_i}{\partial X_I^\beta} &= \frac{1}{\beta X_I^{\beta-1}} \frac{\partial \mu_i}{\partial X_I} \end{aligned} \tag{42}$$

for $X_I > 0$, we can calculate the relationship between the fractal time rate of change and the second order fractal displacement gradients.

By substitution of (40) into (42) and assuming $\zeta = \alpha$ and $\beta = \nu$, it can be shown that

$$\frac{\partial \mu_j}{\partial t^\alpha} = \Sigma_0 \frac{\partial}{\partial X_I^\nu} \left(\frac{\partial \mu_j}{\partial X_I^\nu} \right) = \Sigma_0 \frac{\partial F^\beta_{jI}}{\partial X_I^\nu}. \tag{43}$$

This result gives a strong indication that if the fractal deformation gradient follows a stretched exponential in space and time, a fractal diffusion equation can accurately describe its behavior. Importantly, we use this result to suggest that fractal time derivatives are ideal for modeling viscoelasticity if the material displacements follow stretched exponential distributions. This is counter to

Journal of Applied Mechanics. Received March 27, 2023;
Accepted manuscript posted April 15, 2023. doi:10.1115/1.4062389

prior work that focused on fractional time derivatives to describe viscoelasticity in elastomers [14]. We support this argument in the following section by showing that fractal and fractional order operators give nearly identical viscoelastic stress predictions in both elastomers VHB 4910 and 4949.

4 EXPERIMENTAL VALIDATION

Stress-stretch experiments on the dielectric elastomer Very High Bond(VHB) 4910 and 4949 manufactured by 3M are used to validate the model. A series of uniaxial cyclic loading/unloading stress/stretch tests were conducted to observe the change in steady-state hysteretic stress behavior while varying the stretch rate. Details on the experimental methods can be found elsewhere [35]. These stress/stretch results are used to compare a fractal order linear viscoelastic model to the fractional order viscoelastic model discussed here.

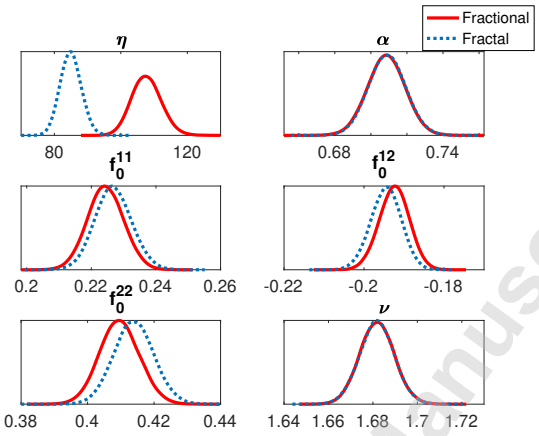

Fig. 2: Overlaid posterior densities of the fractional and fractal order models for VHB 4910 when calibrated a stretch rate corresponding to 0.67 Hz. The red solid lines represent the results for the fractional order model and the blue dotted lines represent the results for the fractal order model.

We further explain fractional order viscoelasticity using the Caputo fractional order derivative (32) to clarify how it is compared to experiments. The integer derivative of the function was previously given by $f^{(n)}(s)$. In our case, the integer derivative of the deformation gradient (F_{iK}) or the stretch rate ($\dot{\lambda}_I$) replaces the function ($f^{(n)}(s)$) and the Caputo fractional order derivative simplifies to

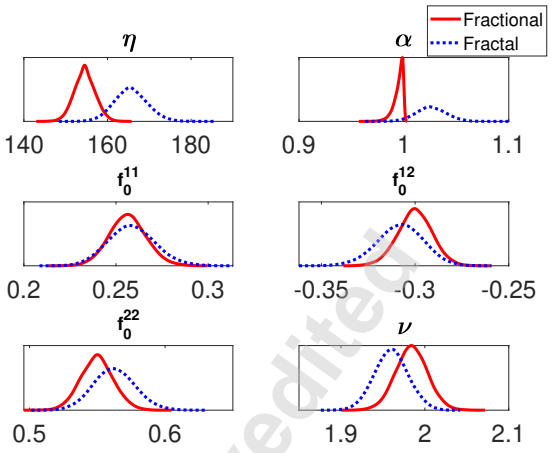

Fig. 3: Overlaid posterior densities of the fractional and fractal order models for VHB 4949 when calibrated at 0.67 Hz. The red solid lines represent the results for the fractional order model and the blue dotted lines represent the results for the fractal order model

$$(D_t^\alpha \lambda_I)(t) = \frac{t^{1-\alpha}}{1-\alpha}\frac{\dot{\lambda}_I}{\Gamma(1-\alpha)} \tag{44}$$

$$\text{for } 0 < \alpha \leq 1$$

where $\alpha > 0$ is the fractional order of the derivative, $\dot{\lambda}_I$ is the constant stretch rate, and the Gamma function has also been given by $\Gamma(n-\alpha)$.

The fractal derivative, on the other hand, is defined by

$$\frac{d\lambda_I}{dt^\alpha} = \frac{t^{1-\alpha}}{\alpha}\frac{d\lambda_I(t)}{dt} \tag{45}$$

where $\alpha > 0$ is the fractal order of the derivative, and $\frac{d\lambda_I(t)}{dt}$ is the integer order derivative of $\lambda_I(t)$. In this simple case, the fractional and fractal deformation gradients are almost equivalent (aside from a factor of $\frac{\alpha}{(1-\alpha)\Gamma(1-\alpha)}$) and the viscoelastic stress/stretch rate relation looks to follow power law behavior. However, in computations dealing with more complicated cases, the solution for the fractional order derivative may not be numerically efficient to compute making the fractal order derivative a suitable alternative.

Journal of Applied Mechanics. Received March 27, 2023;
Accepted manuscript posted April 15, 2023. doi:10.1115/1.4062389

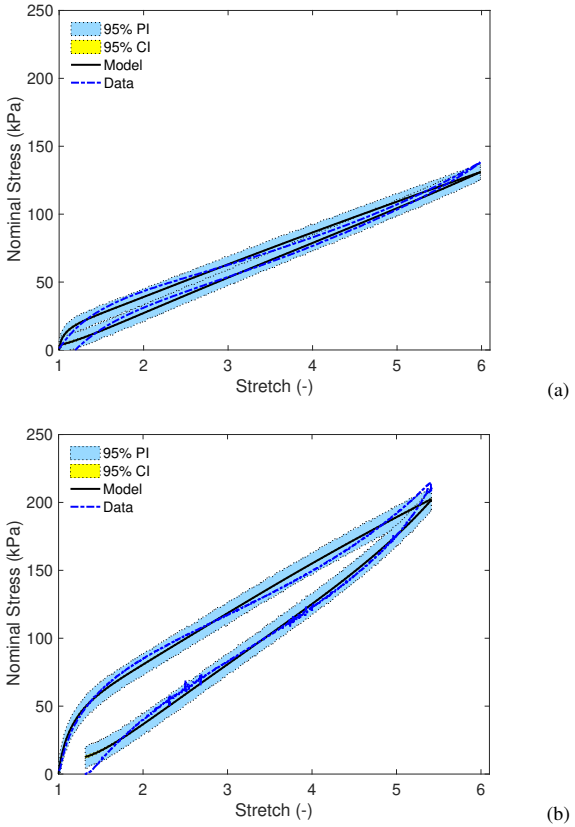

Fig. 4: Fractional Order Model. Representative set of calibration plots for the fractional order model describing the steady-state cyclic stress vs stretch behavior for VHB 4910 at (a) 6.7×10^{-5} Hz, and (b) 0.67 Hz.

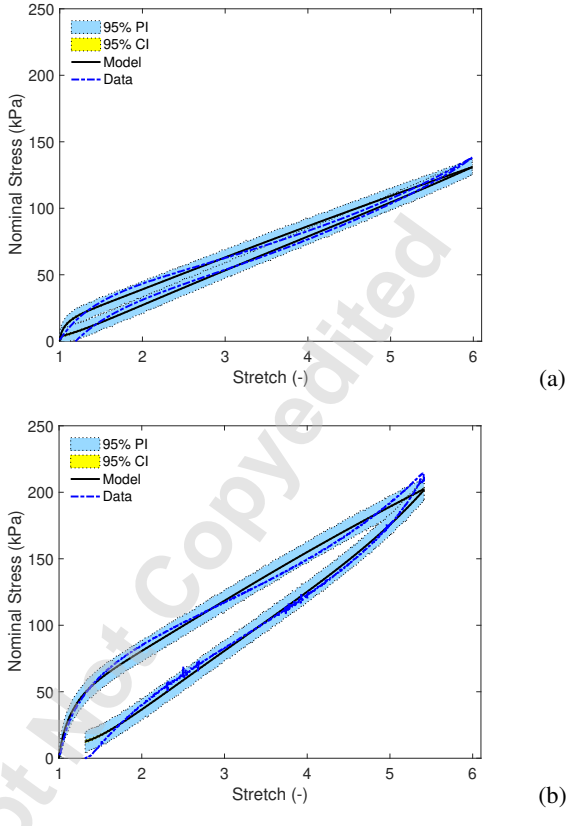

Fig. 5: Fractal Order Model. Representative set of calibration plots for the fractal order model describing the steady-state cyclic stress vs stretch behavior of VHB 4910 at (a) 6.7×10^{-5} Hz and (b) 0.67 Hz.

To describe the total stress, we assume the free energy function has the form given in (25) plus an incompressibility constraint which involves the additional free energy component

$$\hat{\psi} = \psi - p_h(J^{\beta,x} - 1) \tag{46}$$

where $J^{\beta,x} = \lambda_1^{\beta,x}\lambda_2^{\beta,x}\lambda_3^{\beta,x}$ and p_h is an unknown hydrostatic pressure. We are then able to obtain the total hyperelastic stress

$$\begin{aligned} s_L^{tot} &= \frac{\partial\hat{\psi}}{\partial\lambda_L^{\beta,x}} \\ &= T\left[\nu f_0^{11}(\lambda_L^{\beta,x})^{\nu/2-1}\lambda_L^{\beta,x} \right. \\ &\qquad \left. + \nu f_0^{12}(\lambda_L^{\beta,x}\lambda_L^{\beta,y})^{\nu/2-1}\lambda_L^{\beta,y}\right] - p_h\frac{\partial J^{\beta,x}}{\partial\lambda_L^{\beta,x}}. \end{aligned} \tag{47}$$

and solve for the hydrostatic pressure given the zero transverse stress constraint ($s_1^{tot} = s_2^{tot} = 0$) and s_3^{tot} is the uniaxial stress to obtain following pressure equation

$$p_h = \frac{T\left[\nu f_0^{11}(I_1^{11})^{\nu/2-1}\lambda_1^{\beta,x} + \nu f_0^{12}(I_1^{12})^{\nu/2-1}\lambda_1^{\beta,y}\right]}{\lambda_2^{\beta,x}\lambda_3^{\beta,x}} \tag{48}$$

where $I_1^{11} = \lambda_L^{\beta,x}\lambda_L^{\beta,x}$, $I_1^{12} = \lambda_L^{\beta,x}\lambda_L^{\beta,y}$, and $I_1^{22} = \lambda_L^{\beta,y}\lambda_L^{\beta,y}$.

The viscoelastic stress from the unobservable deformation gradient, Γ_{iK}^{β}, can be solved by combining the first and second laws of thermodynamics to describe the irreversible deformation processes with negligible ther-

Journal of Applied Mechanics. Received March 27, 2023;
Accepted manuscript posted April 15, 2023. doi:10.1115/1.4062389

mal gradients. This results in an entropy generation

$$s_g = -\frac{\partial \hat{\psi}}{\partial \Gamma^{\beta}_{iK}}(D^{\alpha}_t \Gamma^{\beta}_{iK})(t) = Q_{iK}(D^{\alpha}_t \Gamma^{\beta}_{iK})(t) \geq 0 \tag{49}$$

or

$$s_g = -\frac{\partial \hat{\psi}}{\partial \Gamma^{\beta}_{iK}}\left(\frac{d\Gamma^{\beta}_{iK}}{dt^{\alpha}}\right) = Q_{iK}\left(\frac{d\Gamma^{\beta}_{iK}}{dt^{\alpha}}\right) \geq 0, \tag{50}$$

depending on whether the fractional or fractal order derivative is used, respectively, where S_g is the entropy generation and irreversibilities are contained in the viscoelastic stress relation $Q_{iK} = -\frac{\partial \hat{\psi}}{\partial \Gamma^{\beta}_{iK}}$. A detailed explanation of how fractional viscoelastic stress in (49) is derived is provided elsewhere [31].

The total stress can then be solved by combining (47), (48), and either (49) or (50) depending on whether the fractal or fractional order derivative, respectively, is being used.

Using Bayesian statistical analysis, the parameter set, $\theta = [\eta, \alpha, f_0^{11}, f_0^{12}, f_0^{22}, \nu]$, for both the fractional and fractal viscoelastic models can then be inferred where η and α describe the viscoelastic behavior and f_0^{11}, f_0^{12}, f_0^{22}, and ν describe the hyperelastic model. The Delayed Rejection Adaptive Metropolis (DRAM) algorithm is employed based upon the Markov Chain Monte Carlo (MCMC) sampling technique to construct posterior distributions [36, 37, 38]. All the chains look to have converged to a stable mean with approximately the same statistical distribution along any point in the sample space for about 2.5×10^5 iterations for the fractional and fractal order models. Figure 2 shows the marginal posterior densities for both the fractional and fractal models for VHB 4910 when calibrated at the fastest stretch rate tested. All six parameters look to have a Gaussian distribution and except for η, the parameter distributions overlap almost completely. The difference in the values for η can be explained by the difference in (44) and (45). Similar plots for VHB 4949 are provided in Figure 3.

Mean parameter values can be found in Table 1 for each tested stretch rate. Overall, each parameter set is similar to the one previously discussed where all the parameters except for η have similar values and η is different by the previously discussed factor for the fractional and fractal models.

Using the determined parameter values, a model fit for the VHB 4910 experimental data at the fastest speed tested can be seen in Figures 4(b) and 5(b) along with calculated 95% credible and prediction intervals for the

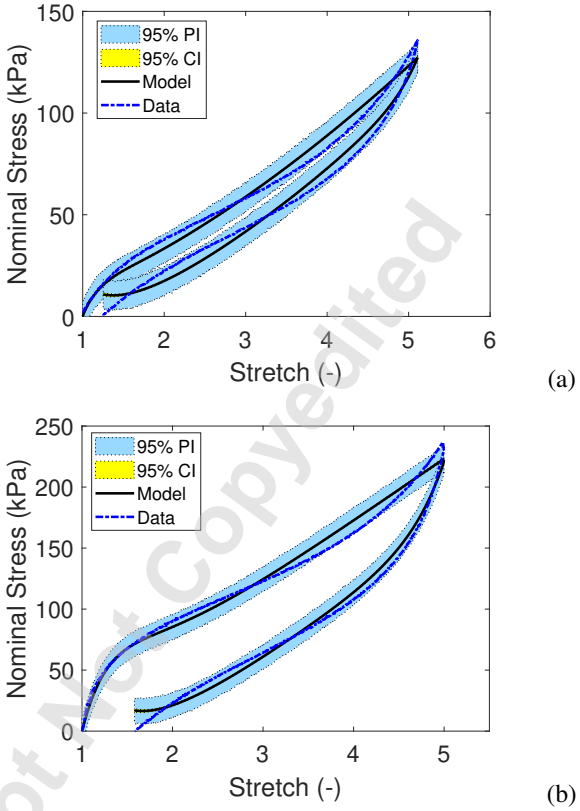

Fig. 6: Fractional Order Model. Representative set of calibration plots for the fractal order model describing the steady-state cyclic stress vs stretch behavior for VHB 4949 at (a) 0.002 Hz, and (b) 0.67 Hz.

Table 1: Mean parameter values for VHB4910 for both the fractional and fractal order models at all calibrated stretch rates.

Model	Parameter	Calibrated Rate (1/s)					
		6.7×10^{-5}	0.047	0.1	0.335	0.5	0.67
Fractional	η	2400	279	194	148	108	108
	α	0.430	0.637	0.657	0.681	0.654	0.709
	f_0^{11}	0.059	0.120	0.144	0.194	0.151	0.224
	f_0^{12}	-0.031	-0.072	-0.089	-0.152	-0.129	-0.193
	f_0^{22}	0.106	0.174	0.200	0.339	0.309	0.410
	ν	1.89	1.72	1.65	1.71	1.84	1.68
Fractal	η	1180	200	143	112	78.9	84.9
	α	0.431	0.637	0.657	0.681	0.654	0.709
	f_0^{11}	0.060	0.121	0.145	0.196	0.153	0.227
	f_0^{12}	-0.032	-0.073	-0.090	-0.154	-0.130	-0.195
	f_0^{22}	0.107	0.176	0.202	0.342	0.312	0.414
	ν	1.89	1.72	1.65	1.71	1.84	1.68

Journal of Applied Mechanics. Received March 27, 2023;
Accepted manuscript posted April 15, 2023. doi:10.1115/1.4062389

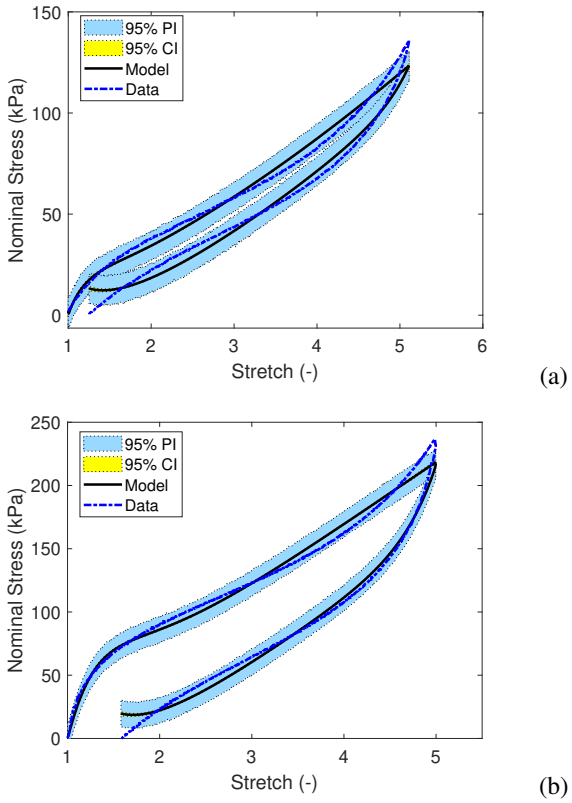

Fig. 7: Fractal Order Model. Representative set of calibration plots for the fractal order model describing the steady-state cyclic stress vs stretch behavior for VHB 4949 at (a) 0.002 Hz, and (b) 0.67 Hz.

Table 2: Mean parameter values for VHB 4949 for both the fractional and fractal order models at all calibrated stretch rates.

Model	Parameter	Calibrated Rate (1/s)				
		0.002	0.02	0.2	0.4	0.67
Fractional	η	6528	1364	307	182	155
	α	0.917	0.965	0.985	0.983	0.995
	f_0^{11}	0.043	0.054	0.148	0.183	0.256
	f_0^{12}	-0.041	-0.057	-0.167	-0.21	-0.3
	f_0^{22}	0.083	0.115	0.312	0.388	0.55
	ν	2.366	2.407	2.095	2.047	1.984
Fractal	η	6350	1419	326	190	166
	α	0.908	0.971	1.003	0.991	1.026
	f_0^{11}	0.043	0.051	0.144	0.177	0.259
	f_0^{12}	-0.043	-0.056	-0.165	-0.208	-0.308
	f_0^{22}	0.092	0.114	0.308	0.387	0.563
	ν	2.32	2.396	2.083	2.032	1.96

fractional and fractal order models, respectively. The same procedure is then used to obtain separate parameter sets for each tested rate. The calibrated model fits at 6.7×10^{-5} can be found in Figures 4(a) for the fractional order model and Figure 5(a) for the fractal order model. The fits between both models look to be almost identical at each tested rate. The fractional and fractal model fit on VHB 4949 data are provided in Figure 6 and Figure 7, respectively, and mean model parameters for both models are listed in Table 2.

Table 3: Sum of squares errors (kPa^2) between the collected experimental data (VHB 4910) and the model given the stated calibrated parameter set.

Model	Calibrated Rate (1/s)					
	6.7×10^{-5}	0.047	0.1	0.335	0.5	0.67
Fractional	9.27	7.39	5.68	15.6	26.4	16.6
Fractal	9.26	7.38	5.68	15.5	26.4	16.6

Table 4: Sum of squares errors (kPa^2) between the collected experimental data (VHB 4949) and the model given the stated calibrated parameter set.

Model	Calibrated Rate (1/s)				
	0.002	0.02	0.2	0.4	0.67
Fractional	13.09	16.86	20.14	22.32	27.37
Fractal	13.40	16.70	19.76	22.17	26.99

To more accurately assess the fits of the calibrated plots, a sum-of-squares error between the experimental data and model using the mean parameter values can be determined. Table 3 and 4 give the errors for each calibrated model fit at each stretch rate. Comparing the fractional and fractal errors, we see that the errors are within 0.1% of each other with the fractal order model slightly outperforming the fractional order model 50% of the time.We also note that the mean estimates for η and α converge to consistent values at higher stretch rates. This is because viscoelasticity is more dominant at high stretch rates. The inferred η and α at higher stretch rates are thus more representative of viscoelastic behavior. Moreover,

fixed η and α from higher stretch rates can accurately predict hysteresis at lower stretch rates; see [14].

5 CONCLUSION

A new modeling framework for polymer mechanics has been developed using entropy dynamics. A cost functional that combined Shannon informational entropy with a fractional order constraint of relative particle displacements was introduced to model non-Gaussian deformation processes that often occur in materials that exhibit fractal structure. The fractional order constraint leads to a Bayesian posterior density that is a function of observable and unobservable internal state deformation variables. Through the use of Boltzmann entropy, we obtain a thermodynamic entropy and entropy generation function from the time-varying Bayesian posterior that accommodates nonlinearities associated with fractal or power-law characteristics in both space and time. The Bayesian posterior obtained from this cost function has the form of a stretched exponential which accommodates non-Gaussian deformation for hyperelastic and viscoelastic behavior. Such fat-tailed probabilities are often seen in complex systems that are fractal in nature. While materials have finite length scales and may not follow an exact power-law or fractal structure, Bayesian inference gives an estimate of uncertainty in the model parameters that result from the power-law assumption.

The current study applied fractional and fractal order operators to characterize the viscoelastic behavior of polymers under constant strain rate loading. Under such loading, local fractal time derivatives and nonlocal fractional order time derivatives were shown to be equivalent excluding a multiplicative constant. The two viscoelastic models were calibrated to experimental data from two different polymers and both illustrated equivalent estimates of viscoelasticity over a broad range of deformation rates, indicating their ability to characterize the materials' viscoelastic behavior accurately. This new approach has important implications for providing stronger connections between complex multifractal structure and power-law hyperelastic and viscoelastic properties that can be used to design and optimize polymer-based materials and structures, as traditional linear viscoelastic models may not capture their nonlinear behavior. Further research could explore applying these models to a broader range of polymers and other loading conditions to assess distinctions between model predictions of data when using local fractal or nonlocal fractional order operators. The study highlights the potential of fractional and fractal order models to advance our understanding of complex material behavior.

ACKNOWLEDGEMENTS

W.S.O. and B.R.P. appreciate support from the Department of Defense Basic Research Program for HBCU/MI (W911NF-19-S-0009). E.L.S. acknowledges support from the DOD SMART Scholarship. The research of S. M. was partially supported by the National Science Foundation grant DBI 2109990. Any opinions, findings, and conclusions or recommendations expressed in this publication are those of the authors and do not necessarily reflect the views of the funding sponsors.

REFERENCES

[1] Malvern, L., 1969, *Introduction to the Mechanics of a Continuous Medium* Prentice-Hall, Inc., Englewood Cliffs, NJ.

[2] Holzapfel, G., 2000, *Nonlinear Solid Mechanics* John Wiley & Sons, Inc., Chichester.

[3] Weiner, J. H., 1983, *Statistical Mechanics of Elasticity* John Wiley & Sons, New York.

[4] Shannon, C. E., 1948, "A mathematical theory of communication," *The Bell system technical journal,* **27**(3), pp. 379–423.

[5] Jaynes, E., 2003, *Probability Theory: The Logic of Science* Cambridge University Press, Cambridge.

[6] Jaynes, E. T., 1957, "Information theory and statistical mechanics," *Phys. Rev.,* **106**, May, pp. 620–630.

[7] Feder, J., 2013, *Fractals* Springer Science & Business Media.

[8] Caticha, A., 2015, "Entropic dynamics," *Entropy,* **17**(9), pp. 6110–6128.

[9] West, B. J., and Grigolini, P., 2010, *Complex webs: anticipating the improbable* Cambridge University Press.

[10] He, J.-H., 2014, "A tutorial review on fractal spacetime and fractional calculus," *International Journal of Theoretical Physics,* **53**(11), June, pp. 3698–3718.

[11] Havlin, S., and Ben-Avraham, D., 1987, "Diffusion in disordered media," *Advances in physics,* **36**(6), pp. 695–798.

[12] Giona, M., Cerbelli, S., and Roman, H., 1992, "Fractional diffusion equation and relaxation in complex viscoelastic materials," *Physica A: Statistical Mechanics and its Applications,* **191**(1-4), Dec., pp. 449–453.

[13] Mainardi, F., Luchko, Y., and Pagnini, G., 2007, "The fundamental solution of the space-time fractional diffusion equation," *arXiv preprint cond-mat/0702419*.

[14] Mashayekhi, S., Hussaini, M. Y., and Oates, W.,

2019, "A physical interpretation of fractional viscoelasticity based on the fractal structure of media: Theory and experimental validation," *Journal of the Mechanics and Physics of Solids,* **128**, pp. 137–150.

[15] Ostoja-Starzewski, M., Li, J., Joumaa, H., and Demmie, P. N., 2014, "From fractal media to continuum mechanics," *ZAMM-Journal of Applied Mathematics and Mechanics/Zeitschrift für Angewandte Mathematik und Mechanik,* **94**(5), pp. 373–401.

[16] Wheatcraft, S. W., and Tyler, S. W., 1988, "An explanation of scale-dependent dispersivity in heterogeneous aquifers using concepts of fractal geometry," *Water Resources Research,* **24**(4), p. 566–578.

[17] Tatom, F. B., 1995, "The between fractional calculus and fractals," *Fractals,* **03**(01), Mar., pp. 217–229.

[18] Rocco, A., and West, B. J., 1999, "Fractional calculus and the evolution of fractal phenomena," *Physica A: Statistical Mechanics and its Applications,* **265**(3-4), Apr., pp. 535–546.

[19] Atangana, A., 2017, "Fractal-fractional differentiation and integration: Connecting fractal calculus and fractional calculus to predict complex system," *Chaos, Solitons & Fractals,* **102**, Sept., pp. 396–406.

[20] Carpinteri, A., and Mainardi, F., 1997, *Fractals and fractional calculus in continuum mechanics* Springer.

[21] Mandelbrot, B. B., Evertsz, C. J., and Gutzwiller, M. C., 2004, *Fractals and chaos: the Mandelbrot set and beyond*, Vol. 3 Springer.

[22] Tarasov, V. E., 2014, "Anisotropic fractal media by vector calculus in non-integer dimensional space," *Journal of Mathematical Physics,* **55**(8), p. 083510.

[23] Balankin, A. S., 2015, "A continuum framework for mechanics of fractal materials i: from fractional space to continuum with fractal metric," *The European Physical Journal B,* **88**(4), pp. 1–13.

[24] Rubinstein, M., and Colby, R., 2003, *Polymer Physics* Oxford University Press, Oxford.

[25] Davidson, J., and Goulbourne, N., 2006, "A non-affine network model for elastomers undergoing finite deformations," J. Mech. Phys. Solids, **61**(8), pp. 1784–1797.

[26] Wheatcraft, S. W., and Meerschaert, M. M., 2008, "Fractional conservation of mass," *Advances in Water Resources,* **31**(10), pp. 1377–1381.

[27] Tarasov, V. E., 2011, *Fractional dynamics: applications of fractional calculus to dynamics of particles, fields and media* Springer Science & Business Media.

[28] Oates, W., Stanisaukis, E., Pahari, B. R., and Mashayekhi, S., 2021, "Entropy dynamics approach to fractional order mechanics with applications to elastomers," In Behavior and Mechanics of Multifunctional Materials XV, R. L. Harne, ed., Vol. 11589, International Society for Optics and Photonics, SPIE, pp. 23 – 34.

[29] Pahari, B. R., and Oates, W., 2022, "Renyi entropy and fractional order mechanics for predicting complex mechanics of materials," In Behavior and Mechanics of Multifunctional Materials XVI, Vol. 12044, SPIE, pp. 49–57.

[30] Jaynes, E. T., 1965, "Gibbs vs. Boltzmann entropies," *American Journal of Physics,* **33**(5), pp. 391–398.

[31] Stanisauskis, E., Mashayekhi, S., Pahari, B., Mehnert, M., Steinmann, P., and Oates, W., 2022, "Fractional and fractal order effects in soft elastomers: Strain rate and temperature dependent nonlinear mechanics," *Mechanics of Materials*, p. 104390.

[32] Havlin, S., and Ben-Avraham, D., 1987, "Diffusion in disordered media," *Advances in physics,* **36**(6), pp. 695–798.

[33] Odibat, Z. M., and Shawagfeh, N. T., 2007, "Generalized taylor's formula," *Applied Mathematics and Computation,* **186**(1), pp. 286–293.

[34] Falconer, K., 2004, *Fractal geometry: mathematical foundations and applications* John Wiley & Sons.

[35] Miles, P., Hays, M., Smith, R., and Oates, W., 2015, "Bayesian uncertainty analysis of finite deformation viscoelasticity," *Mechanics of Materials,* **91**, pp. 35–49.

[36] Haario, H., Saksman, E., and Tamminen, J., 2001, "An adaptive metropolis algorithm," *Bernoulli,* **7**(2), Apr., pp. 223–242.

[37] Haario, H., Laine, M., Mira, A., and Saksman, E., 2006, "DRAM: Efficient adaptive MCMC," *Statistics and Computing,* **16**(4), Dec., pp. 339–354.

[38] Smith, R., 2013, *Uncertainty quantification : theory, implementation, and applications* Society for Industrial and Applied Mathematics, Philadelphia.